Quantum Chemical Study on the Decomposition of N_2O with O^-, O_2^-, and O_3^-

Elly J. Karlsen[†] and Lars G. M. Pettersson*[,‡]

Oil and Energy Research Centre Porsgrunn, Section for Hydrocarbon Processes and Catalysis, Norsk Hydro ASA, N-3907 Porsgrunn, Norway, and FYSIKUM, AlbaNova, Stockholm University, S-106 91 Stockholm, Sweden

Received: October 18, 2002; In Final Form: January 9, 2003

High-level quantum chemical calculations have been performed on the decomposition reactions of N_2O with cation-stabilized oxygen species (O^-, O_2^-, and O_3^-), which compose a model catalytic cycle where O_2^- is regenerated. The calculated results show that O^- and O_3^- can be expected to be the most active species in the N_2O decomposition process, with activation barriers at the multiconfigurational second-order perturbation level (CASPT2) of 29.5 and 32.5 kcal/mol, respectively. The calculated activation barrier for N_2O decomposition through reaction with O_2^- is 40.8 kcal/mol. Comparison with experiments involving these species on metal-oxide substrates indicates the role of the ionic surface to reduce the barriers.

Introduction

The superoxide (O_2^-) species formed on metal oxides has been suggested to play an important role as an intermediate in heterogeneous catalysis on materials such as metal oxides and zeolites. O_2^- may be formed by adsorption of molecular oxygen on, e.g., charged vacancies (F_s and F_s^+ centers), transition metal doped insulating metal oxides, and reducible metal oxides. Pacchioni et al. showed that when O_2 interacts with charged oxygen vacancies, this superoxide may be formed.[1] Moreover, these centers seem to play an active role in heterogeneous catalysis at low temperature.[2] The O_2^- species was shown to be formed through a charge transfer from the F_s center to the adsorbed O_2 and is stabilized on the surface due to the electrostatic interaction with the resulting positively charged surface site. The interaction was found to be strong enough to make this charge-transfer process exothermic. In the decomposition process of N_2O, O_2^- has been proposed to form through abstraction of oxygen from N_2O. The following steps can be outlined, where steps 3 and 4 comprise a catalytic cycle

$$N_2O + e^- \rightarrow N_2 + O^- \quad (1)$$

$$N_2O + O^- \rightarrow N_2 + O_2^- \quad (2)$$

$$N_2O + O_2^- \rightarrow N_2 + O_3^- \quad (3)$$

$$N_2O + O_3^- \rightarrow N_2 + O_2 + O_2^- \quad (4)$$

O_2^- and ozone anion (O_3^-) have been observed in previous studies using electron paramagnetic resonance spectroscopy (EPR) at relatively low temperatures (up to 303 K) when N_2O was interacting with ZrO_2.[3] Even though O^- was not directly observed, it was suggested that this anion is formed in the first step in the decomposition process, in which there is a charge transfer from the surface to the adsorbate. The activation barrier for step 3 was estimated to be as low as about 5 kcal/mol. In transition metal exchanged zeolites, O^- can be formed, for instance in the formation of a $Cu^{2+}-O^-$ pair in Cu/ZSM-5.[4,5] Tuyen et al. have also observed O_3^- for the N_2O decomposition on Pd/ZrO_2 in their EPR study.[6] They suggested that this anion is gradually decomposed to O_2^-. Because both O_2^- and O_3^- have thus been observed experimentally, it is important to consider these species when discussing mechanisms for N_2O decomposition. Moreover, the activation barrier for the formation of O_3^- from O_2^- and N_2O is considered to be very low, which would make O_2^- of potential interest in catalytic N_2O conversion. The low activation barrier becomes particularly interesting in the light of tail-gas applications in, e.g., nitric acid production, where the temperature is relatively low (250−500 °C).

Most of the previous works have focused on the formation of O_2^-, whereas its activity or its role in the whole catalytic cycle has not been considered. In the present work, we will focus on the activity of O_2^- in the N_2O decomposition process, and in particular, we will consider mechanisms in which O^- and O_3^- species are involved in the decomposition process.

Computational Details

The Model. In the present study, we have considered the interaction of N_2O with O^-, O_2^-, and O_3^-. To stabilize these anions with the correct electronic structure, we have used KO, KO_2, and KO_3 as models for O^-, O_2^-, and O_3^- bonded to a surface. All of these complexes are known to exist as ion pairs (K^+O^-, $K^+O_2^-$, and $K^+O_3^-$). Both KO_2 and KO_3 exist as a triangular C_{2v} symmetry structure with the ground spin state as a doublet[7−10] (see Figure 1). Moreover, Alcami et al.[10] have, in a theoretical work, predicted three isomer structures of Li^+O_3 that all lie close in energy. In addition to the C_{2v} (see structure 2 in Figure 1), other isomer structures could exist. One corresponds to the attachment of the alkali metal ion to one of the terminal oxygen atoms, and the other corresponds to insertion of the alkali metal ion in one of the O−O bonds (see structures 3 and 4 in Figure 1). Because the isomer structure 4 does not contain an O_3 unit, it will not be considered further in the present study.

Methods. In the decomposition reaction proposed above, ozone anion is included as one of the intermediates. The

* Author to whom correspondence should be addressed: lgm@physto.se.
† Oil and Energy Research Centre Porsgrunn.
‡ Stockholm University.

10.1021/jp027245d CCC: $25.00
Published on Web 02/13/2003

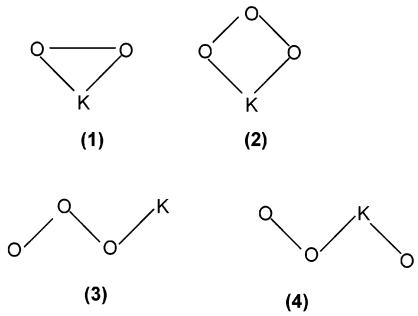

Figure 1. Structures of KO_2 and the three isomeric structures of KO_3.

electronic structure of ozone can be viewed as a mixture of ionic and diradical components, which makes this species and its anion difficult to describe theoretically. Studies of the electron affinity and the dissociation and atomization energies of ozone show that both dynamical and nondynamical correlation effects have to be included to obtain the correct energies.[11,12]

There exist no experimental data or theoretically predicted values on the reaction energies for the decomposition process including the catalytic cycle; therefore, they have been computed in the present work. To assess the accuracy of our calculated values, we have performed test calculations on the species in the cycle and compared our results with experimental data. These benchmark calculations were performed using both the (PCI-80) parametrized configuration interaction[13−15] and multiconfigurational second-order perturbation (CASPT2)[16] methods in single-point calculations at the optimized geometries. In the PCI-80 scheme, the correlation energy is scaled by a basis set and method-dependent parameter obtained from benchmark calculations on light elements and second-row transition metals. The correlation effect obtained in these calculations was about 80%. By application of this scaling scheme, it has been shown that, by, e.g., using a single-reference method like the modified coupled-pair functional (MCPF) method with only a double zeta-polarization (DZP) contracted Gaussian basis set, the average absolute deviation from experiment was drastically improved.[13−15] In the CASPT2 method, the dynamical correlation effect is obtained from second-order perturbation theory using a multiconfiguration wave function as reference. The active space for the transition state structures and N_2O consists of the 2p-derived orbitals for both oxygen and nitrogen, which form lone pairs, π-bonding, and antibonding combinations. Because there is an almost complete charge transfer from the potassium atom to O, O_2, and O_3, there is, in principle, no need to include orbitals derived from potassium in the active space, but the potassium 4s orbital was still included. Thus, for the cation stabilized oxygen anion species, in addition to the 4s orbital, 2p-derived orbitals for oxygen forming π-bonding (in O_2^- and O_3^-) and lone pairs are included in the active space. For KO, the active space in the complete active space self-consistent field (CASSCF) calculation consisted of five electrons distributed among six orbitals (which we denote as 5/6). For KO_2, the CASSCF wave function was generated from an active space containing seven electrons distributed among seven orbitals (7/7). For KO_3, the active space contained nine electrons distributed among eight orbitals (9/8). For all the transition state structures in the reactions with N_2O, we followed the procedure stated above, giving 15/11, 17/12, and 19/13 CASSCF active spaces for the first, second, and third steps, respectively. In the subsequent CASPT2 calculations, the electrons in the 1s orbitals on oxygen and nitrogen as well as the electrons in the 1s, 2s, and 2p orbitals on potassium were not correlated. The geometries of reactants and products were optimized at the density-functional theory (DFT) level with the B3LYP functional using the Gaussian 98[17] program, unless otherwise noted, the basis set used for all atoms in the B3LYP calculations is the 6-311G-(3df,3pd) valence triple-ζ basis set, containing both diffuse and polarization functions. In the CASPT2 calculations, we have used a (14s9p4d3f)[6s5p3d2f] atomic natural orbital (ANO) basis set for both nitrogen and oxygen,[18] while for potassium the basis set was [14s11p5d1f]/(8s7p3d1f). In the PCI-80 scheme, the scaling was done based on the MCPF method for dynamical correlation. The PCI-80 scaling scheme is performed by adding 20% of the correlation effect to the total energy. The Hartree−Fock limit has been included in these calculations, which were performed using the STOCKHOLM set of programs.[19] The Gaussian basis sets used here were (25s18p6d4f)/[9s9p6d4f][7,20] for potassium, while for oxygen the ANO primitive (13s9p6d4f) basis set was contracted to [5s5p2d1f]. For nitrogen, we employ a (14s9p4d3f)[6s5p3d2f] ANO basis set.[7]

Results and Discussion

The results from the present work are divided into three parts. We will first give results on the geometry of O^-, O_2^-, and O_3^- bonded to potassium. Because there are no available experimental data on the reaction energies for the two reaction steps of specific interest for the N_2O decomposition (steps 3 and 4), an evaluation in terms of benchmark calculations of reaction energies involving the species included in these steps is performed and compared with experimental data. The last part of this work will be devoted to the reaction energies, transition state structures, and activation barriers for all the steps in the decomposition process, including the catalytic cycle.

Geometries of KO, KO_2, and KO_3. The bonding in KO can be characterized in terms of an ionic description K^+O^-, but the ground-state symmetry has been a matter of debate in both theoretical and experimental studies. The electron hole on oxygen can give either a $2p\sigma^2 2p\pi^3$ or $2p\sigma^1 2p\pi^4$ configuration resulting in $^2\Pi$ and $^2\Sigma^+$ molecular states, repectively. Langhoff et al. have, in an extensive theoretical study of the $^2\Pi-^2\Sigma^+$ energy separation in KO, shown that the $^2\Sigma^+$ is the ground state.[29] In a recent work by Lee et al., high-level quantum chemical methods have been employed, including relativistic effects (spin−orbit coupling).[21] They concluded that the low-lying states of KO are affected by spin−orbit coupling that leads to an avoided crossing between the $^2\Sigma^+_{1/2}$ and $^2\Pi_{1/2}$ states. At short K−O bond distance, the state is designated as $^2\Sigma^+_{1/2}$, while at long distance $^2\Pi_{1/2}$. For intermediate distances, the character is mixed. The effect on R_e is negligible, however, with a calculated bond distance of 2.19 Å. In calculations without relativistic effects (this scheme is employed in the present work), the energy separation and ground-state determination were found to be more sensitive to the basis set used than to the description of electron correlation. Inclusion of f-functions is particularly important to describe the $^2\Sigma^+$ state properly, while d-functions are more important for the $^2\Pi$ state; not including d- and f-functions will thus have a large effect on the $^2\Pi-^2\Sigma^+$ energy separation. This basis set effect is also investigated in the present work. In optimizing the geometry of KO (B3LYP level), we can clearly see that the ground-state symmetry is dependent on whether we have included f-functions or not (on both K and O). We obtain a ground state of Π-symmetry with a K−O bond length of 2.40 Å in agreement with the results of Langhoff et al. by using a basis set without f-functions. (Dunnings (9s5p1d)/[4s3p1d] augmented with a diffuse p-function with an orbital exponent of 0.059 for oxygen. For potassium, the basis set is of the form (14s10p1d)/[8s4p1d].) An extended triple-ζ basis

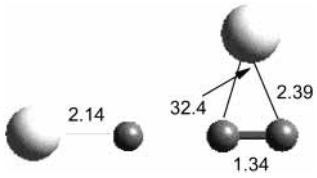

Figure 2. Optimized B3LYP level geometry of KO and KO_2. Bond distances are given in Å, and the angles are given in degrees.

set (6-311G(3df,3pd)) for K and O yields the $^2\Sigma^+$ ground state with a K−O bond length of 2.14 Å. Langhoff et al. used a basis set near the Hartree−Fock (HF) limit and reported single and double excitation configuration interaction model CI-SD and HF level K−O bond lengths of 2.33, 2.35 AA and 2.19, 2.22 AA Å for $^2\Pi$ and $^2\Sigma^+$, respectively. Considering the rather shallow potential energy curves in the KO interaction, the agreement for the geometries is satisfactory.

KO_2 is known from both experimental[8] and theoretical studies,[7] where it has been found to exist in a triangular C_{2v} structure. The electronic ground state is $^2A_2$, which corresponds to charge transfer from potassium to the π^* orbital of molecular dioxygen. The crystallographic value for the O−O bond reported by Tremblay et al.[8] is 1.33 Å. Because KO_2 exists as an ion pair, the O_2 stretching frequency in KO_2 is found, experimentally, to be almost identical to that of the O_2^- anion in the gas phase.[8] As a good approximation, the gas-phase O_2^- bond distance can be used as well. The O−O bond length calculated here (1.336 Å) is in good agreement with both the crystallographic and the gas-phase values for the bond length of O_2^- (1.341 ± 0.010 Å).[22] The K−O bond length is, in all previous theoretical works, determined to be too long (2.39−2.46 Å)[23,24,29] compared to the experimentally determined value of 2.28 Å. These calculations include methods on different levels of theory, like HF, Moeller−Plesset second-order perturbation theory (MP2), B3LYP and quadratic configuration interaction with single and double excitation (QCISD) and MCPF and high-quality basis sets. Our calculated K−O B3LYP level bond length of 2.39 Å is thus in accordance with previous theoretical works and underlines the disagreement between theory and experiment for this structural parameter. The O−K−O angle is here determined to be 32.4°, in good agreement with previous theoretical works (31.1−33.3°) and the crystallographic value of 33.0°.[8] The optimized geometry is shown in Figure 2.

KO_3. Alkali-metal ozonides such as $K^+O_3^-$ have also been studied experimentally. These ozonides are formed by reaction of alkali atoms with ozone. Like in KO_2, there is a complete transfer of the potassium 4s valence electron to the lowest unoccupied molecular orbital ($2b_1$), resulting in $^2B_1$ as the electronic ground state for the $K^+O_3^-$ complex. It has been shown both experimentally and theoretically that the O−O−O bond angle in ozone is slightly smaller in the presence of the alkali metal. Our optimized O−O−O angle in KO_3 is 114.8°, whereas in O_3, the calculated angle is 118.0°. The experimentally determined value for the angle in O_3^- is 111.8 ± 2.0°.[25] Borowski et al. have obtained an O−O−O angle of 115.4° at the CASPT2 level.[26] The O−O bond distance remains almost unaffected compared to ozone, however. The experimentally determined O−O bond distance of ozone is 1.34 ± 0.03 Å,[26,27] while we obtain an O−O bond distance in KO_3 of 1.36 Å. As for the bond distance in KO, there exists no experimental estimate for the gas-phase structure of KO_3. In crystalline KO_3, the K−O distance has been found to be 2.70 Å.[28] We can compare with LiO_3, which has been studied theoretically previously, giving a Li−O bond distance between 2.21 and 2.24 Å. Because potassium has a more electropositive character and its ion has a larger radius, the K−O bond distance should be longer, which we indeed find is the case; r(K−O) is calculated to be 2.46 Å. A structural isomer, with a more open geometry (see Figure 1, structure 3), is calculated to be 14.8 kcal/mol less stable than the ozone structure. However, as will be discussed below, this isomer is the product of the second reaction step, and in addition, no transition state was found for step 3 using the ozone structure. The calculated geometries of both isomer structures are given in Figure 3.

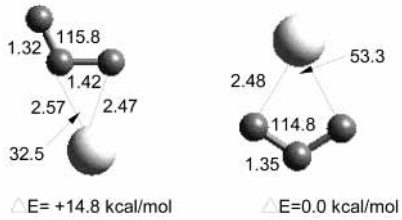

Figure 3. Optimized B3LYP level structures of the two KO_3 isomers with the ozone related structure on the right. Bond distances are given in Å, and the angles are given in degrees.

TABLE 1: Reaction Energies (kcal/mol) Calculated at Different Levels of Theory and Compared with Experimental Data

reactions	PCI-80	CASPT2	expt
$O_3 \rightarrow 3O$	155.5	145.5	144.6[a]
$O_3^- \rightarrow O_2 + O^-$	46.0	35.6	35.9[a,b,c]
$O_3^- \rightarrow 2O + O^-$	168.4	152.6	154.9[a,b,c]
$O_2 + e \rightarrow O_2^-$	3.2	7.6	9.9[e]
$O + e \rightarrow O^-$	−29.8	−31.7	−33.7[c]
$O_3 + e \rightarrow O_3^-$	39.7	50.0	48.5[b]
$KO_2 \rightarrow K + O_2$	40.7	38.2	40.6 ± 7[d]
$2N_2O \rightarrow 2N_2 + O_2$	−41.4	−38.0	−39.2[a]

[a] Reference 30. [b] Reference 31. [c] Reference 32. [d] Reference 33. [e] Reference 34.

Benchmark Calculations. There exist no experimental data or theoretically predicted values for the reaction energies in the decomposition reaction steps. To evaluate our calculated values, test calculations on the species in this cycle have been performed and compared with experimental data. In Table 1, our computed results for a set of reactions containing the more problematic molecules are given with results achieved with both the PCI-80 scaling scheme and the CASPT2 method. For the alkali-metal superoxide bond energy, the dissociation energy is determined using the scheme of Langhoff et al.,[7,29] in which the dissociation energy is computed relative to the dissociated ion fragments. The energy is then adjusted to the ground-state neutral fragments by using the experimentally determined electron affinity for O_2 and the potassium ionization potential. By this approach, one avoids problems in accurately determining the electron affinity of O_2. As the result in Table 1 shows, the calculated electron affinity deviates by 2.3 kcal/mol at the CASPT2 level. The results for superoxide bond energy using the PCI-80 scaling scheme and CASPT2 are in very good agreement with experiment. The MCPF method accounts for most of the correlation effects for systems that can be well described by a single-reference wave function, which is the case for ionic systems such as KO_2. Moreover, the correlation contribution to the binding energy, when computed relative to the dissociated ionic species, is only 2.3 kcal/mol.

For problematic molecules such as the ozone ion, the deficiency of the single-determinant MCPF method in describing near-degeneracies becomes prominent. Single-determinant methods tend to overestimate the correlation energy in such cases as can be seen from Table 1, in which the dissociation energies

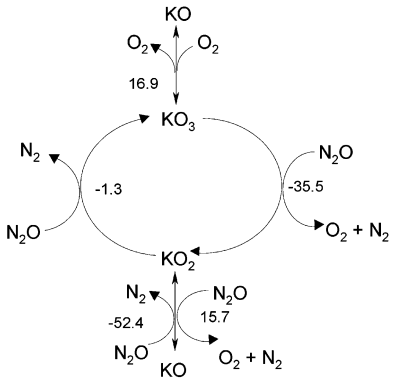

Figure 4. Reaction energies (kcal/mol) for the steps in the N_2O decomposition reaction. The reaction energies have been calculated at the CASPT2 level.

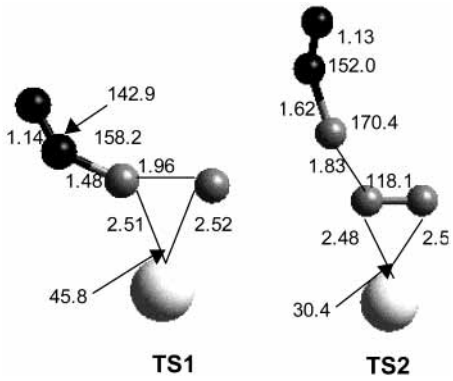

Figure 5. Optimized structures of transition states. **TS1** is the transition state for the first reaction step, while **TS2** is for the second step in the catalytic cycle. Bond distances are given in Å, and the bond angles are given in degrees. The potassium atom is colored white, oxygen is gray, and nitrogen is black.

of ozone and ozone ion are overestimated relative to experiment by 10.9, 10.1, 13.5, and 8.8 kcal/mol, respectively. Because ozone ion is present in the catalytic cycle, it is necessary to calibrate the reaction energies using the CASPT2 method, in which both nondynamical and dynamical correlation effects are included. The latter part is described through a second-order perturbation approach, in which the CASSCF wave function is used as a reference. Including both near-degeneracy effects and the dynamical correlation using this technique leads to a mean absolute deviation from the experimental values, which is now reduced to 0.3−2.3 kcal/mol in all reactions in which ozone, or its anion, is included. Thus, the computational procedure for determination of the energetics of the steps in the N_2O decomposition reaction will rely on a B3LYP geometry optimization combined with a CASPT2 single-point calculation to obtain accurate reaction energies

The Catalytic Cycle. The reaction energies and activation barriers for all the reaction steps including steps 3 and 4 in the catalytic cycle have been computed using the DFT method with the B3LYP functional for the geometry optimization. The character of each transition state has been confirmed by performing a vibrational frequency analysis. Because the CASPT2 method is capable of describing the more complex species like ozone more correctly, only this method has been used in single-point calculations at the equilibrium and transition-state geometries. The results are displayed in Figure 4 and the geometries of the transition-state structures are given in Figure 5 and Figure 6.

As can be seen from the results in Figure 4, the first reaction step is highly exothermic, with a reaction energy of 52.4 kcal/

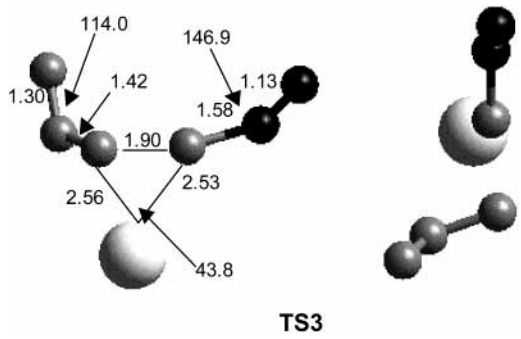

Figure 6. Optimized structures of transition states. **TS3** is the transition state for the third reaction step. Bond distances are given in Å and the bond angles are given in degrees. The potassium atom is colored white, oxygen is gray, and nitrogen is black.

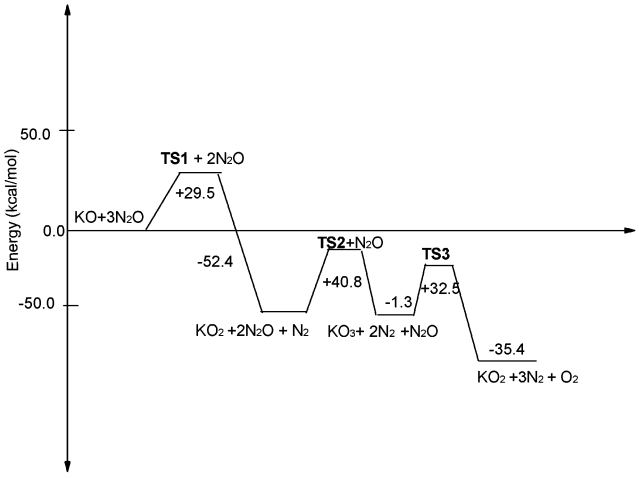

Figure 7. Schematic potential curve of the N_2O decomposition reaction over potassium oxides.

mol. A high reaction energy (59.3 kcal/mol) has also been obtained in the work by Lu et al. on N_2O decomposition over Li-doped MgO.[35] The second step, leading to formation of an ozone anion, is thermoneutral (−1.3 kcal/mol), while the regeneration step is exothermic by 35.5 kcal/mol. Alternative routes are also given. Because the regeneration of the KO structure from KO_2 with N_2O is endothermic by about 16 kcal/mol, this step can most likely be ruled out. The same can be concluded for the regeneration of the KO structure from KO_3. However, the reverse reaction suggests that, in the presence of O_2, formation of KO_3 directly from KO is possible. The **TS1** and **TS2** structures are given in Figure 5, while **TS3** is displayed in Figure 6. The potential curve is schematically given in Figure 7. For the **TS1** and **TS3** structures, the N−O bond is less elongated than that for the **TS2** structure. The higher degree of activation of the N−O bond in **TS2** is reflected in the higher activation barrier for this step (40.8 kcal/mol) compared to steps 1 (29.5 kcal/mol) and 3 (32.5 kcal/mol). Moreover, the NNO−O distance is longer for the **TS1** and **TS3** structures. Analysis of the Mulliken populations shows a slightly higher degree of charge transfer from the substrate to N_2O in the first and second steps ($\Delta q = -0.3$ vs $\Delta q = -0.2$ for step 2). This charge transfer from the potassium oxides to the π^* orbital of N_2O causes a more bent N_2O geometry for all the transition-state structures.

The relatively high activation barrier of step 2 combined with a thermoneutral reaction energy suggests that O_2^- interaction with N_2O is not favorable at low temperatures, which is in contradiction to the experimental results.[3] It is important, however, to underline the fact that we have not included the effect of the surface in the present calculations. Because the

surface is not included, we are not able to evaluate the effect of the surface on the relative stabilization of the oxygen anion species and transition-state structure or the effect of possible high coverage of formed surface superoxides and ozonides. The effect of surface coverage will most likely be important when considering the stabilization of these formed intermediates and of the transition state structures. Moreover, an increased surface coverage of the formed intermediates could also open other reaction pathways, e.g., in the regeneration of the active sites. It is most likely that the TS structures become more stabilized as a result of electrostatic interactions with the ionic substrate. This effect has, for instance, been demonstrated in previous theoretical work on N_2O decomposition over alkaline-earth oxides.[36,37] For low surface coverage, we have shown that there is a stabilization of the transition-state structure due to electrostatic fit of the adsorbate to the underlying surface. However, an increased surface peroxide coverage leads to a dramatic decrease in the stabilization of the transition state structure and, thereby, an increase of the activation barrier.[36] On the other hand, it has previously been shown that the stabilization of formed surface peroxides is reduced upon increased surface peroxide coverage.[38] Increased superoxide coverage could also result in alternative pathways for formation of ozonide and regeneration of the active sites

$$2O_2^- \rightarrow O_2 + 2O^- \quad (5)$$

$$2O_2^- \rightarrow 2O^- + O_3^- \quad (6)$$

The first step is endothermic for cation-stabilized models by almost 37 kcal/mol. The second step is highly exothermic (58.2 kcal/mol) and could be an alternative route for formation of ozonide and regeneration of the active site. Moreover, in EPR studies on MgO and Pd/ZrO, O_3^- has been shown to gradually decompose to O_2^- .[6,39] An alternative route for ozonide ion decomposition could be formation of molecular oxygen

$$2O_3^- \rightarrow 2O^- + O_2 \quad (7)$$

which is also calculated to be exothermic (28.5 kcal/mol). So, for increased coverage of surface oxygen anion species, different reaction routes for regeneration of the reactive surface species may be thermodynamically feasible. This may also hold from the kinetic point of view; that is, some of these alternative pathways could also give a lower activation barrier compared to the reactions involving N_2O for the regeneration of the active site.

Finally, for transition-metal-based catalysts, it is possible that the electron-transfer process is accomplished by overlap of orbitals with suitable energy and symmetry between the substrate (e.g., d-orbitals on the transition metal) and N_2O. All in all, the catalytic surface, also including surface intermediates formed, is most likely directly involved in the activation of N_2O in addition to playing a more direct role in the stabilization of the formed intermediates and regeneration of the active sites.

Conclusions

Quantum chemical calculations have been performed on N_2O decomposition over oxygen species, which have been proposed to play an important role in catalysis over, e.g., metal oxides. The first reaction step where O_2^- is formed is highly exothermic, with the lowest activation barrier in the N_2O decomposition process (29.5 kcal/mol). O_2^- is much less active toward N_2O decomposition with the largest activation barrier, and the reaction is only thermoneutral. The regeneration step in which O_2^- is formed is exothermic by 35.4 kcal/mol, and the calculated activation barrier is close to that of the first step. These results based on gas-phase models of the active species are in contradiction with experiments on transition-metal oxides, and we conclude that the direct involvement of the surface for the stabilization of the intermediates is crucial; this needs to be taken into account in order to strictly analyze the surface reactions. The inherent electronic structure and reactivity properties associated with these oxygen anionic species play an important role, but the present results demonstrate that the surface plays a decisive role in stabilizing the activated species at the transition state. Moreover, high surface coverage of the formed intermediates could be important in determining the relative stabilization of these intermediates in addition to having a direct effect on the stabilization of the transition state. Finally, we should not exclude the possibility of other reaction pathways for regeneration of the surface, i.e., by recombination of the surface intermediates.

Acknowledgment. All the calculations were performed on the HPC Superdome machine in Oslo. The computer facility at USIT, University of Oslo, is organized under the NOTUR program, which is partly funded by the Norwegian Research Council. The generous grant of CPU time is hereby acknowledged, and we thank the staff at USIT for technical support.

References and Notes

(1) Pacchioni, G.; Ferrari, A. M.; Giamello, E. *Chem. Phys. Lett*. **1996**, *255*, 58.
(2) Valentin, C. D.; Pacchioni, G.; Abbet, S.; Heiz, U. *J. Phys. Chem. B* **2002**, *106*, 7666−7673.
(3) Aika, K.; Iwamatsu, E. *Stud. Surf. Sci. Catal.* **1994**, *90*, 195.
(4) Giamello, E.; Lamberti, C.; Palomino, G. T.; Fisicaro, P.; Bordiga, S.; Zecchina, A. *J. Phys. Chem. B* **2000**, 4064−4073.
(5) Trout, B. L.; Chakraborty, A. K.; Bell, A. T. J. *Phys. Chem*. **1996**, *100*, 4173−4179.
(6) Tuyen, N van; Ikonnikov, I. A.; Loginov, A. Yu.; Romanovskii, B. V. *Kinet. Catal.* **1997**, *38*, 94.
(7) Partridge, H.; Bauschlicher, C. W., Jr.; Sodupe, M.; Langhoff, S. R. *Chem. Phys. Lett.* **1992**, *195*, 200.
(8) Tremblay, B.; Manceron, L.; Roy, P.; LeQuere, A. M.; Roy, D. *Chem. Phys. Lett.* **1994**, *228*, 410.
(9) Andrews, L.; Spiker, R. C., Jr. *J. Chem. Phys*. **1972**, *59*, 1851.
(10) Alcami, M.; Cooper, I. L.; Mo, O.; Yanez, M. *Chem. Phys*. **1995**, *103*, 253.
(11) Gonzalez-Luque, R.; Merchan, M.; Borowski, P.; Roos, B. O. *Theor. Chim. Acta* **1993**, *86*, 467.
(12) Borowski, P.; Roos, B. O.; Racine, S. C.; Lee, T. J.; Carter, S. *J. Chem. Phys*. **1995**, *1*, 103.
(13) Siegbahn, P. E. M.; Blomberg, M. R. A.; Svensson, M. *Chem. Phys. Lett*. **1994**, *23*, 35.
(14) Blomberg, M. R. A.; Siegbahn, P. E. M.; Svensson, M. *J. Chem. Phys*. **1996**, *104*, 9546.
(15) Siegbahn, P. E. M.; Svensson, M.; Boussard, P. J. E. *J. Chem. Phys.* **1995**, *102*, 5377.
(16) Andersson, K.; Blomberg, M. R. A.; Fülscher, M. P.; Karlström, G.; Lindh, R.; Malmquist, P. Å.; Neogrády, P. J.; Olsen, J.; Roos, B. O.; Sadlej, A. J.; Schúltz, M.; Seijo, L.; Serrano-Andrés, L.; Siegbahn, P. E. M.; Widmark, P. O.; MOLCAS-5, Lund University, Sweden, 2001.
(17) Frisch, M. J.; Trucks, G. W.; Schlegel, H. B.; Scuseria, G. E.; Robb, M. A.; Cheeseman, J. R.; Zakrzewski, V. G.; Montgomery, J. A., Jr.; Stratmann, R. E.; Burant, J. C.; Dapprich, S.; Millam, J. M.; Daniels, A. D.; Kudin, K. N.; Strain, M. C.; Farkas, O.; Tomasi, J.; Barone, V.; Cossi, M.; Cammi, R.; Mennucci, B.; Pomelli, C.; Adamo, C.; Clifford, S.; Ochterski, J.; Petersson, G. A.; Ayala, P. Y.; Cui, Q.; Morokuma, K.; Malick, D. K.; Rabuck, A. D.; Raghavachari, K.; Foresman, J. B.; Cioslowski, J.; Ortiz, J. V.; Stefanov, B. B.; Liu, G.; Liashenko, A.; Piskorz, P.; Komaromi, I.; Gomperts, R.; Martin, R. L.; Fox, D. J.; Keith, T.; Al-Laham, M. A.; Peng, C. Y.; Nanayakkara, A.; Gonzalez, C.; Challacombe, M.; Gill, P. M. W.; Johnson, B. G.; Chen, W.; Wong, M. W.; Andres, J. L.; Head-Gordon, M.; Replogle, E. S.; Pople, J. A. *Gaussian 98*, revision A.9; Gaussian, Inc.: Pittsburgh, PA, 1998.
(18) Bauschlicher C. W., Jr.; Partridge, H. *Chem. Phys*. **1990**, *148*, 57.

(19) STOCKHOLM is a general purpose quantum chemical set of programs written by P. E. M Siegbahn, M. R. A. Blomberg, L. G. M. Pettersson, B. O. Roos, and J. Almlöf.
(20) Partridge, H. *J. Chem. Phys*. **1989**, *90*, 1043.
(21) Lee, E. P. F.; Soldán P.; Wright, T. G. *J. Chem. Phys.* **2002**, *117*, 8241−8247.
(22) Celotta, R. J.; Bennet, R. A.; Hall, J. L.; Siegel, M. W.; Levine, J. *Phys. Rev. A* **1972**, *6*, 631.
(23) Lee, P. F.; Wright, T. G. *J. Phys. Chem. A* **1998**, *102*, 1036.
(24) Lee, E. P. F.; Wright, T. G. *Chem. Phys. Lett*. **2002**, *363*, 139.
(25) Wang, J.; Woo, S. B.; Helmy, E. M. *Phys. Rev. A* **1987**, *35*, 759.
(26) Borowski, P.; Roos, B. O.; Racine, S. C.; Lee, T. J.; Carter, S. *J. Chem. Phys*. **1995**, *1*, 103.
(27) Andrews, R. C.; Spiker, Jr. *J. Chem. Phys.* **1973**, *4*, 59.
(28) Azaroff, L. V.; Corvin, J. *Proc. Natl. Acad. Sci. U.S.A.* **1963**, *49*, 1.
(29) Langhoff, S. R.; Bauschlicher, C. W., Jr.; Partridge, H. *J. Chem. Phys*. **1986**, *84*, 4474.
(30) Chase, M. W., Jr. NIST_JANAF, Thermochemical Tables, 4th ed. In *J. Phys. Chem. Ref. Data*, Monograph 9, **1998**, 1−1951.
(31) Novich, S. E.; Engelking, P. C.; Jones, P. L.; Futrell, J. H.; Lineberger, W. C. *J. Chem. Phys*. **1979**, *70*, 2652.
(32) Neumark, D. M.; Lykke, K. R.; Andersen, T.; Lineberger, W. C. *Phys. Rev. A* **1985**, *32*, 1890.
(33) Jensen, D. E. *J. Chem. Soc., Faraday Trans*. **1982**, *78*, 2835.
(34) Parisel, O.; Ellinger, Y.; Giessner-Prettre, C. *Chem. Phys. Lett.* **1996**, *250*, 178−181.
(35) Lu, X.; Xu, X.; Wang, N.; Zhang, Q. *J. Phys. Chem. B* **1999**, *103*, 3373.
(36) Karlsen, E. J.; Nygren, M. A.; Pettersson, L. G. M. *J. Phys. Chem. A* **2002**, *106*, 7868.
(37) Karlsen, E. J.; Pettersson, L. G. M. *J. Phys. Chem. B* **2002**, *106*, 5719.
(38) Snis, A.; Panas, I. *J. Chem. Phys*. **1995**, *103*, 7626.
(39) Tench, A. J.; Lawson, T. *J. Chem. Soc., Faraday Trans.* **1972**, *68*, 1181.